

Research Article

# Enzyme kinetics from circular dichroism of insulin reveals mechanistic insights into the regulation of insulin-degrading enzyme

Valerie A. Ivancic, Claire A. Krasinski, Qiuchen Zheng, Rebecca J. Meservier,  Donald E. Spratt and  Noel D. Lazo

Carlson School of Chemistry and Biochemistry, Clark University, 950 Main Street, Worcester, MA 01610, U.S.A.

Correspondence: Noel D. Lazo (nlazo@clarku.edu)



Insulin-degrading enzyme (IDE) is a zinc metalloprotease that selectively degrades biologically important substrates associated with type 2 diabetes and Alzheimer's disease (AD). As such, IDE is an attractive target for therapeutic innovations. A major requirement is an understanding of how other molecules present in cells regulate the activity of the enzyme toward insulin, IDE's most important physiologically relevant substrate. Previous kinetic studies of the IDE-dependent degradation of insulin in the presence of potential regulators have used iodinated insulin, a chemical modification that has been shown to alter the biological and biochemical properties of insulin. Here, we present a novel kinetic assay that takes advantage of the loss of helical circular dichroic signals of insulin with IDE-dependent degradation. As proof of concept, the resulting Michaelis–Menten kinetic constants accurately predict the known regulation of IDE by adenosine triphosphate (ATP). Intriguingly, we found that when  $Mg^{2+}$  is present with ATP, the regulation is abolished. The implication of this result for the development of preventative and therapeutic strategies for AD is discussed. We anticipate that the new assay presented here will lead to the identification of other small molecules that regulate the activity of IDE toward insulin.

## Introduction

Insulin-degrading enzyme (IDE) is an attractive target [1,2] for the development of novel therapeutic strategies for type 2 diabetes (T2D) and Alzheimer's disease (AD), because it degrades amylin [1], which self-assembles to form assemblies that are toxic to the insulin-producing pancreatic  $\beta$ -cells [3] and the amyloid- $\beta$  protein ( $A\beta$ ) [2,4], which aggregates to form neurotoxic oligomers [5]. IDE is composed of an N-terminal half (IDE-N) and a C-terminal half (IDE-C) joined by a flexible loop (PDB ID 4PES, Figure 1A) [6,7]. The two halves come together to form a catalytic chamber, also known as a crypt, with a volume of approximately  $16,000 \text{ \AA}^3$ , excluding substrates that contain more than 80 amino acids [6,8–12]. The crypt of IDE also has interesting electrostatic properties in that the predominantly negative interior of IDE-N complements the predominantly positive interior of IDE-C. IDE-N contains a highly conserved exosite (Figure 1A), which has been hypothesized to anchor IDE's substrates prior to degradation [1,8], and the active site ( $\sim 30 \text{ \AA}$  away from the exosite) which contains the  $Zn^{2+}$  binding motif HXXEH (Figure 1B), in which the two histidines (H108 and H112) coordinate  $Zn^{2+}$  and the glutamate residue (E111, replaced by glutamine in 4PES) is directly involved in the hydrolysis of peptide bonds. Replacing E111 with glutamine deactivates IDE [13].

The ability of IDE to degrade amyloidogenic substrates suggests that the development of small-molecule activators that increase its activity is an attractive therapeutic strategy for T2D and AD. However, enhancing the activity of IDE has deleterious consequences. As its name implies, IDE also degrades insulin

Received: 10 August 2018  
Revised: 03 October 2018  
Accepted: 05 October 2018

Accepted Manuscript Online:  
10 October 2018  
Version of Record published:  
07 November 2018

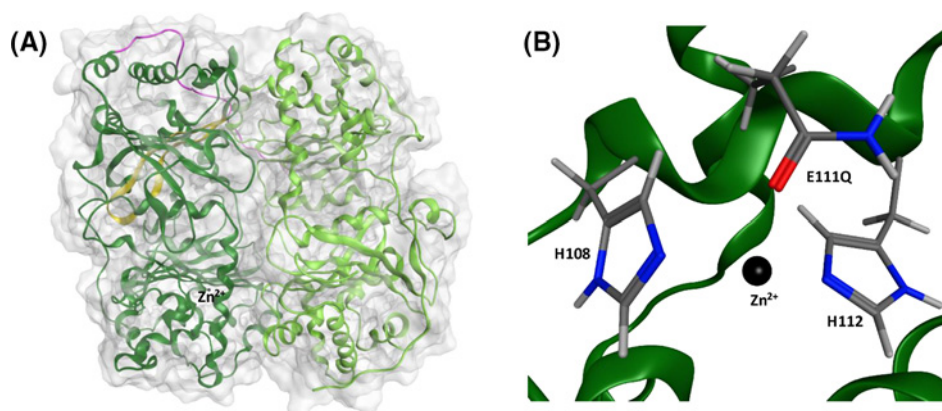


**Figure 1. Structure of IDE determined by X-ray crystallography (PDB ID 4PES [7])**

(A) Molecular surface of IDE along with the ribbon representation of its tertiary structure. IDE is composed of an N-terminal half (IDE-N, dark green) and a C-terminal half (IDE-C, light green) linked by a flexible linker (magenta). IDE-N contains a conserved exosite (yellow) which contains an anti-parallel  $\beta$ -sheet. (B) The active site is found in IDE-N and contains the HXXEH motif, in which the two histidines (H108 and H112) coordinate  $Zn^{2+}$  and the glutamate (E111 mutated to a glutamine in 4PES) participates in the hydrolysis of peptide bonds.

[14,15], a hormone that regulates blood glucose levels by helping cells take in glucose. A more attractive therapeutic strategy, therefore, is one that will enhance the IDE-dependent clearance of the amyloidogenic substrates without offsetting the normal levels of insulin. An important requirement of this strategy is the identification of regulators that govern the activity of the enzyme toward insulin *in vivo*.

Insulin is composed of two chains (A and B), joined together by two interchain disulfide bonds ( $Cys^{A7}-Cys^{B7}$  and  $Cys^{A20}-Cys^{B19}$ ). Previous kinetic studies on the identification of potential regulators of the IDE-dependent degradation of insulin have used the trichloroacetic (TCA) assay [16,17], presumably because of the impracticality of using HPLC for insulin degradation assays, as discussed by Duckworth [18]. The TCA assay, however, requires monoiodination of one of four tyrosines ( $Tyr^{A14}$ ,  $Tyr^{A19}$ ,  $Tyr^{B16}$ , and  $Tyr^{B26}$ ) of insulin, and the location of iodine can affect the kinetics of the degradation [18]. The latter is to be expected, since experimental and theoretical studies have shown that site-specific iodination of insulin modifies its biological and biochemical properties [19]. Quantum mechanical calculations have shown that the positive  $\sigma$ -hole of large halogens including iodine can form stabilizing interactions with proximate water molecules and polar groups [20–22]. Site-specific iodination of  $Tyr^{B26}$  enhances the binding of insulin to its receptor [23,24] and increases the resistance of a rapid acting insulin analog to fibrillation [25]. We hypothesize that the site-specific iodination of insulin also enhances the interaction of the protein with IDE, thus making the relevance of *in vitro* studies that used iodinated insulin to the degradation of insulin *in vivo* difficult to ascertain.

In the present study, we used circular dichroism (CD) to monitor the IDE-dependent degradation of unlabeled insulin. By using the observed ellipticity at 222 nm as a measure of the extent of degradation, we were able to obtain Michaelis–Menten kinetic constants in the absence and presence of adenosine triphosphate (ATP), which has been hypothesized to regulate IDE *in vivo* [10,16,17,26,27]. Our results show that ATP regulates IDE-dependent degradation of insulin, but the addition of  $Mg^{2+}$  abolishes the regulation. Importantly, this finding has implications for the development of therapeutic and/or preventative strategies for AD.

## Materials and methods

### Insulin-degrading enzyme expression and purification

The vector (pGEX-6p-1) encoding glutathione S-transferase tagged human insulin-degrading enzyme (GST-IDE) was kindly provided by Dr Malcolm A. Leissring (University of California, Irvine). The E111Q mutation was introduced into the vector using site-directed mutagenesis and verified by DNA sequencing. Wild-type and E111Q GST-IDE were expressed in *Escherichia coli* BL21 (DE3) codon plus competent cells and grown in LB broth at 37°C to an  $OD_{600}$  of 0.4. Expression was then induced with 50  $\mu$ M isopropyl- $\beta$ -1-thiogalactopyranoside, followed by incubation for 16 h at 200 rpm and 25°C. The cells were harvested by centrifuging at 1500 $\times$ g for 10 min at 4°C.

The pellet was then resuspended in 20 ml PBS with 400  $\mu\text{L}$  of a 100-mM solution of the non-metalloprotease inhibitor phenylmethylsulfonyl fluoride in ethanol. The solution was then homogenized using an Avestin homogenizer to break open the cells, then centrifuged at  $103,000\times g$  for 40 min to separate the cell debris from the soluble protein. The IDE-containing supernatant was syringe filtered with a 0.2  $\mu\text{m}$  filter and purified using a 5 mL GST Trap Fast Flow column (GE) on an ÄKTA Pure FPLC and eluted with PBS containing 10 mM glutathione. Fractions containing IDE were combined and incubated for 1 h at room temperature with 600  $\mu\text{L}$  of GST PreScission protease (2.5 mg/mL) to cleave the GST-tag. The solution was dialyzed overnight in PBS at 4°C with gentle stirring. Purification by size-exclusion chromatography was completed using a HiLoad 16/600 Superdex 200 pg column, also connected to the ÄKTA Pure FPLC. The concentration of the purified protein was determined using UV absorbance at 280 nm ( $\epsilon_{280\text{ nm}} = 113,570\text{ M}^{-1}\text{ cm}^{-1}$  [28]). Glycerol was then added to the solution of IDE to 1% (v/v). After aliquoting, the solutions were flash frozen with liquid nitrogen and stored at  $-80^\circ\text{C}$ .

## Preparation of stock solutions

Human insulin and ATP were purchased from Sigma–Aldrich (St. Louis, MO), and stock solutions of each molecule were prepared in 50 mM Tris buffer (pH 7.4). To overcome the low solubility of insulin at pH 7.4, the solutions were incubated at 37°C overnight, cooled down to room temperature the following day and then centrifuged at  $16000\times g$  for 1 min to remove undissolved protein. Concentrations were determined by UV absorbance at 276 nm ( $\epsilon_{276\text{ nm}} = 6190\text{ M}^{-1}\text{ cm}^{-1}$  [29]) for insulin and by UV absorbance at 259 nm ( $\epsilon_{259\text{ nm}} = 15,400\text{ M}^{-1}\text{ cm}^{-1}$  [30]) for ATP.  $\text{MgCl}_2$  was purchased from Fisher Scientific (Fair Lawn, NJ). Stock solutions of  $\text{MgCl}_2$  at 50 mM were prepared in 50 mM Tris buffer (pH 7.4).

## CD spectroscopy

Far UV CD spectra were recorded at 37°C using a JASCO J-815 spectropolarimeter. Quartz cuvettes with a path length of 1 mm were used. Each spectrum reported in this work was an average of four scans, with each scan recorded from 260 to 198 nm using 1 nm steps and an averaging time of 1 s. All samples were kept at 37°C in between recording of spectra.

## LC/MS

IDE-dependent digestions of insulin were conducted at 37 and at 4°C at a substrate-to-enzyme molar ratio of 100:1. Aliquots (18  $\mu\text{L}$ ) of each digestion were removed periodically and acidified with 8  $\mu\text{L}$  of 1% (v/v) trifluoroacetic acid in water to quench the reactions. To break the disulfide bonds prior to LC/MS, the samples were neutralized and reduced immediately with 10  $\mu\text{L}$  of 45 mM dithiothreitol for 30 min at 50°C. The samples were then alkylated in the dark with 10  $\mu\text{L}$  of 100 mM iodoacetamide for 30 min at room temperature.

All LC/MS experiments were conducted at the Proteomics and Mass Spectrometry Facility of the University of Massachusetts Medical School. After drying the samples, they were diluted to 5  $\mu\text{M}$  in a solution of 5% acetonitrile and 0.1% TFA. Peptide separation and identification by mass spectrometry were achieved using a NanoAcquity UPLC system (Waters Corporation) interfaced to an Orbitrap Q Exactive hybrid mass spectrometer (Thermo Fisher Scientific). The digests were fractionated using an analytical column packed with 25 cm of 3  $\mu\text{m}$  Magic C18AQ (Bruker–Michrom) particles. Solvents A and B were 0.1% formic acid in water and 0.1% formic acid in acetonitrile, respectively. The elution program included a linear gradient developed from 5% solvent A to 35% solvent B in 45 min. Ions were introduced by positive electrospray ionization through a liquid junction into the mass spectrometer. Mass spectra were recorded from 300 to 1750 ( $m/z$ ) at 70,000 resolution ( $m/z$  200). Data-dependent acquisition chose the ten most abundant precursor ions for tandem mass spectrometry by higher energy collisional dissociation using an isolation width of 1.6 Da, collision energy of 27, and a resolution of 17,500.

Raw data files were processed using version 2.1 of Proteome Discoverer (Thermo Fisher Scientific) prior to database searching with version 2.5 of Mascot Server against the *Uniprot\_Human* database. Search parameters did not include enzyme specificity. Variable modifications were considered, including N-terminal acetylation of the protein, oxidized methionine and pyroglutamic acid for N-terminal glutamine. Search results were then loaded into Scaffold Viewer (Proteome Software, Inc.).

## Enzyme kinetics

Seven insulin solutions in 50 mM Tris buffer (pH 7.4), each with a volume of 200  $\mu\text{L}$ , were prepared in Eppendorf tubes. The concentration of the solutions ranged from 15 to 110  $\mu\text{M}$  (15, 20, 25, 30, 50, 80, and 110  $\mu\text{M}$ ). The reaction was initiated with the addition of IDE at a concentration of 1  $\mu\text{M}$ . The solution was then transferred into a 1-mm path

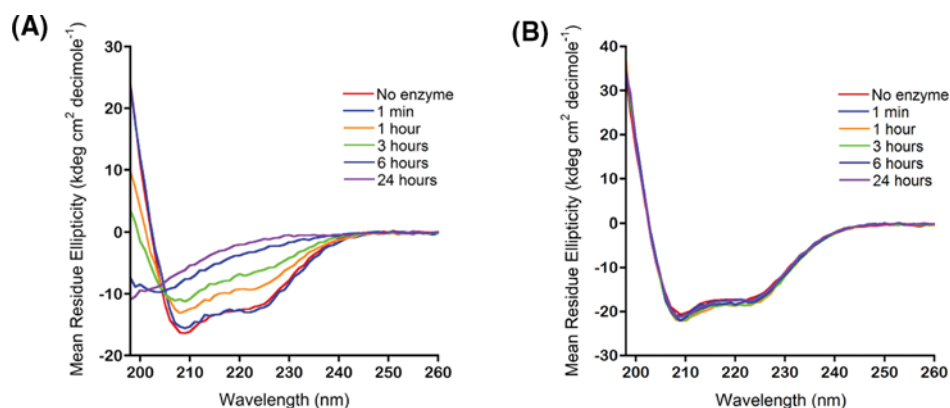


**Figure 2. The far UV CD spectrum of insulin is sensitive to the extent of IDE-dependent degradation**

(A) In the presence of IDE, the helical dichroic signals of insulin at 222 and 208 nm are lost as digestion time is increased from 1 min to 24 h. (B) In the presence of E111Q IDE, the helical dichroic signals of insulin persisted. All spectra in (A) and (B) were collected at 37°C on 20 μM insulin in 50 mM Tris buffer, pH 7.4. The substrate-to-enzyme molar ratio was 100:1.

length quartz cuvette which was then loaded into the sample holder of our CD spectrometer, where the ellipticity at 222 nm ( $[\theta_{\text{obs}}(222 \text{ nm})]$ ) was recorded for 5 min at 37°C. The real-time  $[\theta_{\text{obs}}(222 \text{ nm})]$  data were then used to calculate the amount of digested insulin ([DI]) using (eqn 1). Initial rates ( $V_0$ ) were determined from plots of [DI] against time. Michaelis–Menten, Lineweaver–Burk, and Hanes–Wolf plots were constructed and used to determine the kinetic constants  $K_M$ ,  $V_{\text{max}}$ ,  $k_{\text{cat}}$ , and  $k_{\text{cat}}/K_M$ .

## Results and discussion

Our premise for using CD in our studies of the IDE-dependent degradation of insulin is based on the current working model of the IDE-dependent degradation of insulin [1,8]: the predominantly  $\alpha$ -helical structure of insulin must unfold following its binding and degradation within the crypt of IDE. If true, the  $\alpha$ -helical dichroic spectrum of insulin, showing two negative absorption bands centered at 222 and 208 nm and a positive absorption band centered below 200 nm [31], must change dramatically. Indeed, CD spectra of insulin in the presence of IDE recorded periodically show loss of the helical dichroic signals with increasing digestion time (Figure 2A). In sharp contrast, the dichroic spectrum of insulin did not change in the presence of E111Q IDE (Figure 2B), demonstrating that in the presence of the inactive form of IDE, insulin does not unfold.

To show unambiguously that the loss of helical content in Figure 2A was due to insulin degradation, we performed digestions using conditions similar to those used in preparing the CD samples in Figure 2 (i.e., 20 μM insulin in 50 mM Tris buffer (pH 7.4), substrate-to-enzyme molar ratio of 100:1, digestion temperature of 37°C). Aliquots of the digests were taken periodically for analysis by LC/MS. To unambiguously determine where the cleavages occur, insulin in the quenched digests was reacted with dithiothreitol to reduce Cys residues followed by alkylation using iodoacetamide to prevent the reformation of disulfide bonds. Supplementary Figure S1 presents the mass spectra of the 1-min, 3-h, and 24-h digests. The signals detected in the spectrum of the 1-min digest include peaks corresponding to intact A and B chains and peaks corresponding to two fragments of the A chain, Gly<sup>A1</sup>–Leu<sup>A13</sup> and Tyr<sup>A14</sup>–Asn<sup>A21</sup> (Supplementary Figure S1A, Supplementary Table S1). With an increase in digestion time to 3 h, peaks corresponding to additional fragments were detected along with peaks for intact A and B chains that were of lower intensities relative to the 1-min spectrum (Supplementary Figure S1B and Supplementary Table S1). At 24 h, no peak corresponding to intact A or B was detected, indicating complete degradation of insulin (Supplementary Figure S1C, Supplementary Table S1).

Next, we calculated the well-known Michaelis–Menten kinetic constants using the observed ellipticity at 222 nm ( $[\theta_{\text{obs}}(222 \text{ nm})]$ ). After adding IDE to insulin, we recorded in real time  $[\theta_{\text{obs}}(222 \text{ nm})]$  and observed that the ellipticity increases (i.e., it becomes less negative indicating loss of helical structure [32]) with an increase in digestion time (Figure 3A). Based on the assumption that the increase in  $[\theta_{\text{obs}}(222 \text{ nm})]$  correlates with the amount of insulin digested, we thus used the following equation to approximate the amount of insulin digested over time:

$$[\text{DI}]_t = [\text{I}]_0 \times \left( 1 - \frac{[\theta_{\text{obs}}(222 \text{ nm})]_t}{[\theta_{\text{obs}}(222 \text{ nm})]_0} \right) \quad (1)$$

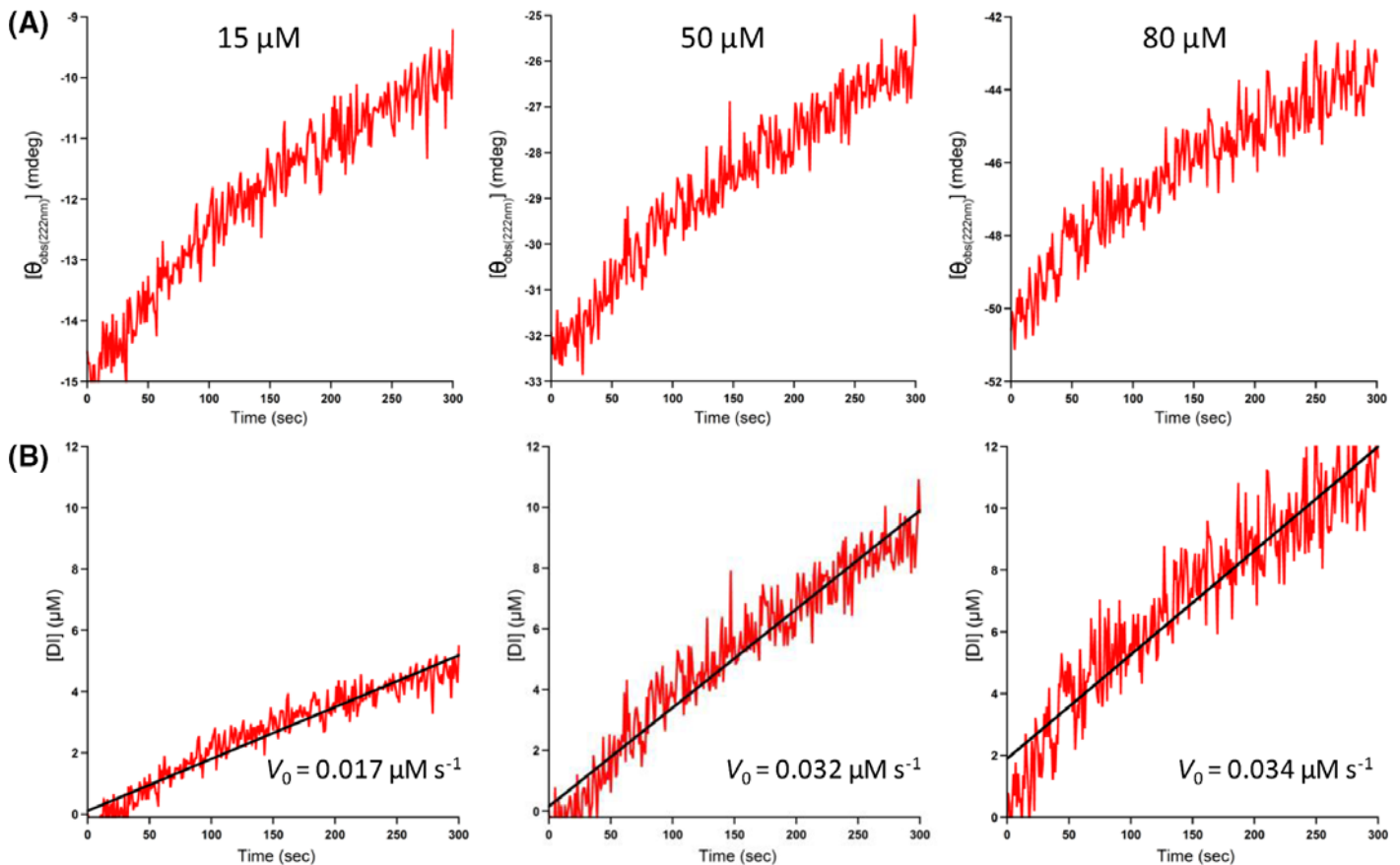


**Figure 3.** Early-stage kinetics of the IDE-dependent degradation of insulin in 50 mM Tris buffer (pH 7.4) at 37°C using observed ellipticity at 222 nm ( $[\theta_{\text{obs}(222 \text{ nm})}]$ )

(A) Representative real-time plots of  $[\theta_{\text{obs}(222 \text{ nm})}]$  versus digestion time (0–300 s). The initial substrate concentration is indicated at the top of each plot. (B) Corresponding real-time plots of digested insulin ([DI]), calculated using eqn 1, versus digestion time. The  $R^2$  values of the fitting of the data to straight lines are (from left to right) 0.92, 0.92, and 0.88. The slope of each line yields  $V_0$ .

**Table 1** Steady-state kinetic parameters<sup>1</sup> for the degradation of insulin by IDE at pH 7.4 and 37°C determined from Michaelis–Menten plots

Regulator	$K_M$ (M)	$k_{\text{cat}}$ ( $\text{s}^{-1}$ )	$k_{\text{cat}}/K_M$ ( $\text{M}^{-1}\text{s}^{-1}$ )
None	$2.0 \pm 0.04 \times 10^{-5}$	$0.048 \pm 0.08$	$2.4 \pm 0.02 \times 10^3$
1 mM ATP	$3.0 \pm 0.2 \times 10^{-5}$	$0.056 \pm 0.2$	$1.8 \pm 0.07 \times 10^3$
1 mM ATP + 1 mM $\text{Mg}^{2+}$	$2.0 \pm 0.05 \times 10^{-5}$	$0.044 \pm 0.07$	$2.1 \pm 0.02 \times 10^3$

<sup>1</sup>Values are the means  $\pm$  S.D. from three trials.

where  $[\text{DI}]_t$  is the amount of insulin digested at time  $t$ ,  $[\text{I}]_0$  is the initial amount of undigested insulin, and  $[\theta_{\text{obs}(222 \text{ nm})}]_t$  and  $[\theta_{\text{obs}(222 \text{ nm})}]_0$  are the observed ellipticities at 222 nm at time  $t$  and time = 0, respectively. We noted that if  $[\theta_{\text{obs}(222 \text{ nm})}]_t$  equals  $[\theta_{\text{obs}(222 \text{ nm})}]_0$ , i.e., there is no change in the ellipticity, (eqn 1) correctly predicts that the amount of digested insulin is 0. Figure 3B presents representative plots of  $[\text{DI}]_t$  against digestion time. Linear regression analysis yields  $V_0$ , the initial velocity (or initial rate) of the IDE-catalyzed degradation of insulin. We used seven initial concentrations of the substrate ([S]) and kept the concentration of IDE constant and determined  $V_0$  from plots similar to Figure 3B. To obtain an initial proof of concept, we constructed Michaelis–Menten, Lineweaver–Burk and Hanes–Wolf plots (Figure 4), and obtained the expected hyperbolic increase in  $V_0$  with an increase in [S], linear increase in  $1/V_0$  with an increase in  $1/[\text{S}]$ , and linear increase in  $[\text{S}]/V_0$  with an increase in [S], respectively. From these plots, we determined the steady-state kinetic parameters  $K_M$ ,  $k_{\text{cat}}$ , and  $k_{\text{cat}}/K_M$ . Table 1 presents the parameters

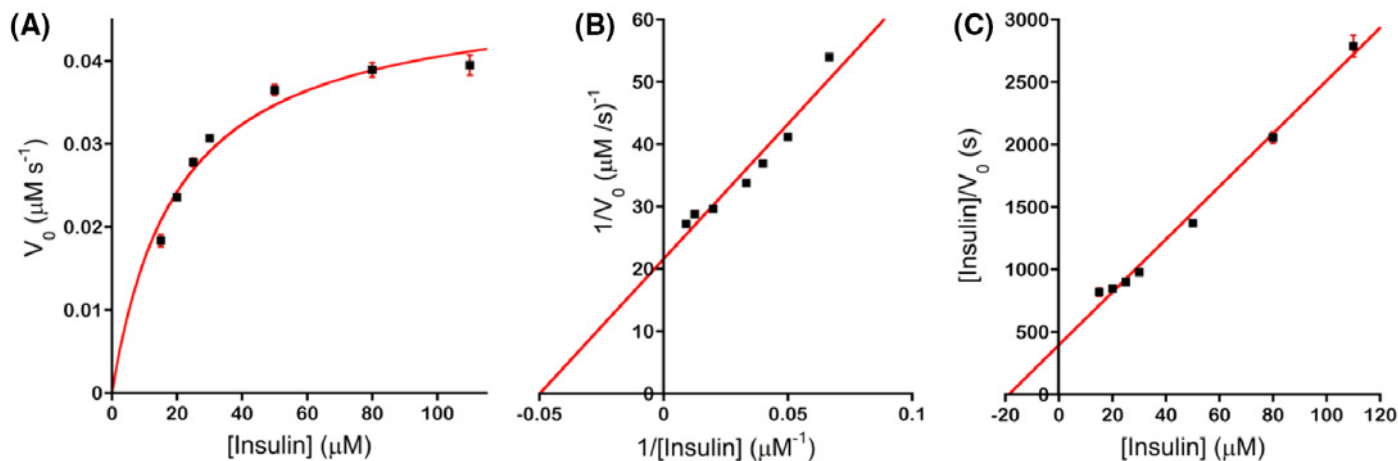


**Figure 4. The IDE-dependent degradation of insulin at pH 7.4 and 37°C follows Michaelis–Menten kinetics**

Kinetic plots including (A) Michaelis–Menten, (B) Lineweaver–Burk, and (C) Hanes–Woolf plots were obtained from  $V_0$  determined from real-time plots of  $[^0_{\text{obs}}(222 \text{ nm})]$  versus digestion time. Each solid square represents the mean of  $V_0$ ,  $1/V_0$ , or  $[\text{insulin}]/V_0$  from three kinetic trials and the error bars represent standard deviations.

determined from the Michaelis–Menten plots. Similar results were obtained from the Lineweaver–Burk (Supplementary Table S2) and Hanes–Woolf (Supplementary Table S3) plots. We noted that the specificity constant  $k_{\text{cat}}/K_M$  of  $2.4 \times 10^3 \text{ M}^{-1} \text{ s}^{-1}$  (Table 1) is less than the value of  $4.0 \times 10^4 \text{ M}^{-1} \text{ s}^{-1}$  determined by Chesneau and Rosner for recombinant human IDE and  $^{125}\text{I}$ -insulin (iodinated at Tyr<sup>A14</sup>) [33]. We speculate that the higher  $k_{\text{cat}}/K_M$  obtained by Chesneau and Rosner is due to an enhancement of the interaction of chain A of insulin with the active site of IDE, resulting in an increased rate of cleavage of the peptide bond between Leu<sup>A13</sup> and Tyr<sup>A14</sup>, the bond that is cleaved initially by IDE as determined by limited proteolysis (LP) (*vide infra*).

To determine the effect of ATP on the IDE-dependent hydrolysis of insulin and to obtain additional proof of concept, we repeated our digestion experiments in the presence of 1 mM ATP and 1 mM ATP plus 1 mM Mg<sup>2+</sup>. Table 1, Supplementary Tables S2 and S3 present the kinetic parameters determined from dichroic data similar to those shown in Figure 3A. Our results show that the addition of 1 mM ATP decreases  $k_{\text{cat}}/K_M$  by 25 % (Table 1, Supplementary Tables S2 and S3), consistent with previous work by Song and co-workers showing that ATP regulates the activity of IDE toward large substrates including insulin [17]. The regulation may be mediated by the electrostatic interaction of the negatively charged triphosphate moiety of ATP with the positively charged interior of IDE-C [10,11]. Additionally, we found that when an equimolar amount of Mg<sup>2+</sup> is present, ATP has no effect on  $k_{\text{cat}}/K_M$  (Table 1, Supplementary Tables S2 and S3), suggesting that the presence of Mg<sup>2+</sup> modulates the electrostatic interaction between ATP and IDE-C. Together, our results provide strong proof of concept for the validity of our CD-based assay.

We noted that the  $k_{\text{cat}}$  of IDE in the absence or presence of ATP is more than two orders of magnitude slower than the median turnover of  $\sim 10 \text{ s}^{-1}$  determined by Bar-Even and co-workers from an analysis of several thousand enzymes and their natural substrates [34], let alone compared with  $k_{\text{cat}}$  of well-known examples of fast enzymes (e.g., superoxide dismutase and carbonic anhydrase), or to the theoretical limit of  $10^6$ – $10^7 \text{ s}^{-1}$  [35]. The  $k_{\text{cat}}/K_M$  of IDE in the absence and presence of ATP is two orders of magnitude smaller than the median  $k_{\text{cat}}/K_M$  of  $\sim 10^5 \text{ M}^{-1} \text{ s}^{-1}$  determined by Bar-Even and co-workers [34]. Together, these observations suggest that IDE, when compared with other enzymes in the literature, is inefficient in degrading insulin. To explain the low  $k_{\text{cat}}$  and  $k_{\text{cat}}/K_M$  of IDE, we noted that it has been hypothesized that IDE is specific to  $\beta$ -structure-forming substrates [1,2,6], presumably because the substrate forms  $\beta$ -sheet-like interactions with IDE prior to degradation [36]. To determine the orientation of insulin in the crypt of IDE during proteolysis, we used LP together with LC/MS. We have previously used LP and LC/MS to successfully elucidate the conformation of monomeric states of amyloidogenic peptides including A $\beta$  [37,38] and amylin [39]. By applying the conditions for LP including substrate-to-enzyme molar ratios  $\geq 100:1$ , digestion temperature of 4°C, and short digestion times ( $\sim 1$  min), the initial cleavage site in insulin can be identified and then used as a constraint in deciphering the arrangement of insulin monomer in the crypt of IDE. Figure 5A presents the mass spectrum of the 1-min digest. Interestingly, the spectrum is similar to the mass spectrum of the 1-min digest at 37°C (Supplementary Figure S1A) in that the peaks detected in the spectrum include peaks corresponding to intact A and

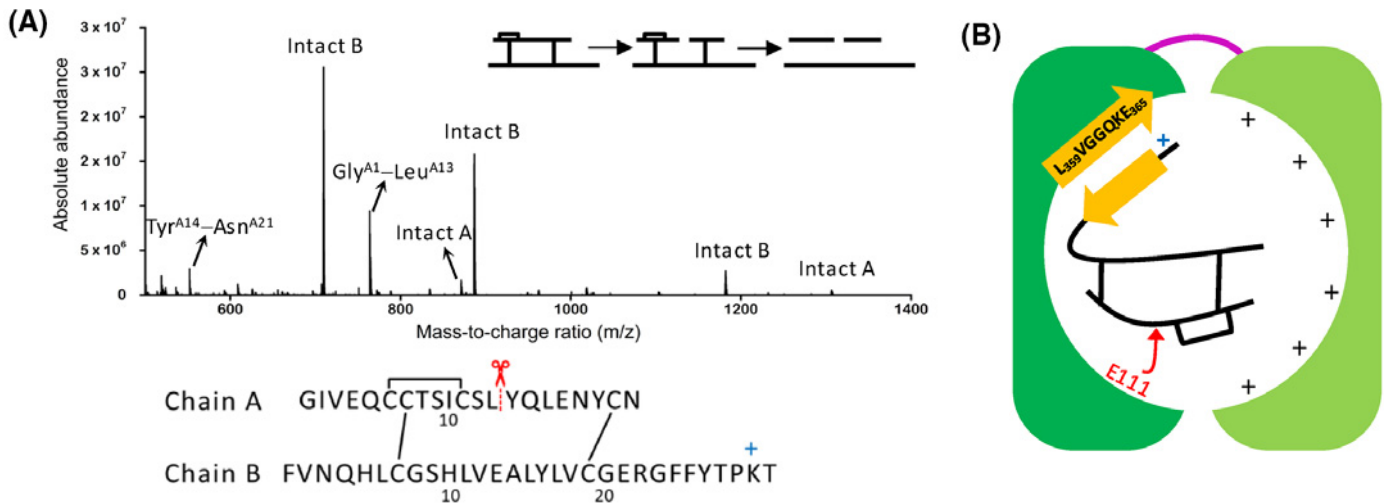


**Figure 5. Limited proteolysis of insulin by IDE**

Insulin (100  $\mu$ M in 50 mM Tris buffer (pH 7.4) was digested at 4°C by IDE using a substrate to enzyme molar ratio of 100:1. Quenched digests were reduced and alkylated for the unambiguous identification of the initial cleavage site by mass spectrometry. (A) Mass spectrum of the 1-min digest. The peaks corresponding to intact A, intact B, Gly<sup>A1</sup>–Leu<sup>A13</sup>, and Tyr<sup>A14</sup>–Asn<sup>A21</sup> are identified. The inset shows schematically how the reduction and alkylation of insulin make possible the unambiguous identification of the initial cleavage site. Below the mass spectrum, the peptide map of insulin shows that the site of the initial cleavage is the peptide bond between Leu<sup>A13</sup> and Tyr<sup>A14</sup>. (B) Schematic representation of the orientation of insulin in the crypt of IDE. IDE-N and IDE-C are shown in dark green and light green, respectively. We hypothesize that the C-terminal segment of chain B of insulin interacts with one of the  $\beta$ -strands in IDE's exosite, mediated in part by the electrostatic interaction between the positively charged lysine residue in the C-terminus of the B chain of insulin (Lys<sup>B29</sup>), and the negatively charged glutamate residue in the exosite of IDE (E365), directing the initial cleavage to take place near the middle of chain A.

B chains and peaks corresponding to fragments of the A chain including Gly<sup>A1</sup>–Leu<sup>A13</sup> and Tyr<sup>A14</sup>–Asn<sup>A21</sup>. This result unambiguously indicates that the initial cleavage occurs in chain A of insulin, particularly at the peptide bond between Leu<sup>A13</sup> and Tyr<sup>A14</sup>. This agrees with the current working model of how IDE sequentially cleaves insulin [8] and with studies of the IDE-dependent hydrolysis of insulin by LC/MS [40] and by matrix assisted laser desorption ionization mass spectrometry [41]. X-ray structures of IDE show that its exosite forms an anti-parallel  $\beta$ -sheet (Figure 1A) consisting of a  $\beta$ -strand (L<sub>359</sub>VGGQKE<sub>365</sub>), a  $\beta$ -turn (G<sub>366</sub>ARG<sub>369</sub>), and a second  $\beta$ -strand (F<sub>370</sub>FFIINV<sub>376</sub>) [7]. The underlined residues are found in the crypt of IDE. The only way for the initial cleavage to occur in chain A of insulin is for the exosite of IDE to bind the C-terminal segment of the B chain of insulin (Figure 5B), not its N-terminus, as previously hypothesized [1,8]. We noted that the C-terminal segment of the B chain of insulin has a high propensity to form  $\beta$ -sheet in that in the structure of insulin dimer [31], the repeating unit in the hexameric form of the protein *in vivo*, the C-terminal segment of the B chain of one monomer forms a  $\beta$ -sheet with the C-terminal segment of the B chain of the other monomer. We speculate that the anchoring of the C-terminal segment of the B chain of insulin to IDE's exosite is facilitated by interactions of the (L<sub>359</sub>VGGQKE<sub>365</sub>)  $\beta$ -strand of IDE with the C-terminal segment of insulin, including an electrostatic attraction between Lys<sup>B29</sup> and E365, thereby directing the initial cleavage to occur in the unstructured middle part of the A chain (Figure 5B). Our model supports the hypothesis that the specificity of IDE to  $\beta$ -structure-forming substrates is due to the interaction of the non-helical part of the substrate with the  $\beta$ -sheet structure of IDE's highly conserved exosite. IDE is slow and inefficient in its turnover of insulin because this substrate is predominantly  $\alpha$ -helical.

How might our results summarized in Table 1 be exploited in the development of therapeutic and/or preventative strategies for AD? Recently, Patel and co-workers showed that ATP at physiological concentrations in the presence of an equimolar amount of Mg<sup>2+</sup> is a biological hydrotrope in that it increases the solubility of proteins and prevents the aggregation of monomers of A $\beta$ 42 [42], one of the most amyloidogenic forms of A $\beta$  [43]. This finding suggests that the ability of IDE to degrade monomeric A $\beta$ 42 may be enhanced in the presence of ATP. Because levels of ATP decline with ageing or mitochondrial impairment [44,45], our results as summarized in Table 1, suggest that preventative

strategies aimed at maintaining the normal levels of ATP and  $Mg^{2+}$  may boost the IDE-dependent clearance of A $\beta$ 42 without offsetting the normal levels of insulin.

In conclusion, we have presented a novel assay for the determination of Michaelis–Menten kinetic constants for the IDE-dependent degradation of unlabeled insulin. We anticipate that this assay will inform us of other small molecules that regulate the degradation of insulin. A full understanding of the IDE-dependent degradation of insulin is key in the development of therapeutic strategies targeting IDE to treat T2D and AD.

## Acknowledgement

We thank Prof. Malcolm A. Leissring of the University of California at Irvine for his generous assistance in the production of IDE.

## Author contribution

V.A.I. and C.A.K. produced IDE under the guidance of D.E.S.; V.A.I. obtained CD spectra and analyzed MS data; V.A.I., C.A.K., Q.Z., and R.J.M. obtained and analyzed kinetic data; V.A.I. wrote the first draft of the manuscript, V.A.I. and Q.Z. made figures and tables, and all authors contributed to the editing process; N.D.L. designed and supervised the study and the writing of the manuscript.

## Funding

This work was supported by the National Institute on Aging of the National Institutes of Health through the [grant number R15AG055043] awarded (to N.D.L.). Preliminary parts of this work were funded by an internal grant awarded to N.D.L. by the Lise Ann and Leo Beavers II endowment to Clark University.

## Competing interests

The authors declare that there are no competing interests associated with the manuscript.

## Abbreviations

A $\beta$ , amyloid- $\beta$ ; AD, Alzheimer's disease; ATP, adenosine triphosphate; CD, circular dichroism; FPLC, fast protein liquid chromatography; GST-IDE, glutathione-S-transferase tagged human insulin-degrading enzyme; IDE, insulin-degrading enzyme; IDE-C, C-terminal half of IDE; IDE-N, N-terminal half of IDE; LP, limited proteolysis; TCA, trichloroacetic acid; T2D, type 2 diabetes; UPLC, ultra performance liquid chromatography.

## References

- Tang, W.J. (2016) Targeting insulin-degrading enzyme to treat type 2 diabetes mellitus. *Trends Endocrinol. Metab.* **27**, 24–34, <https://doi.org/10.1016/j.tem.2015.11.003>
- Kurochkin, I.V., Guarnera, E. and Berezovsky, I.N. (2018) Insulin-degrading enzyme in the fight against Alzheimer's disease. *Trends Pharmacol. Sci.* **39**, 49–58, <https://doi.org/10.1016/j.tips.2017.10.008>
- Lorenzo, A., Razzaboni, B., Weir, G.C. and Yankner, B.A. (1994) Pancreatic islet cell toxicity of amylin associated with type-2 diabetes mellitus. *Nature* **368**, 756–760, <https://doi.org/10.1038/368756a0>
- Saido, T. and Leissring, M.A. (2012) Proteolytic degradation of amyloid  $\beta$ -protein. *Cold Spring Harb. Perspect. Med.* **2**, a006379, <https://doi.org/10.1101/cshperspect.a006379>
- Cline, E.N., Bicca, M.A., Viola, K.L. and Klein, W.L. (2018) The amyloid- $\beta$  oligomer hypothesis: Beginning of the third decade. *J. Alzheimer's Dis.* **64**, S567–S610, <https://doi.org/10.3233/JAD-179941>
- Shen, Y., Joachimiak, A., Rosner, M.R. and Tang, W.J. (2006) Structures of human insulin-degrading enzyme reveal a new substrate recognition mechanism. *Nature* **443**, 870–874, <https://doi.org/10.1038/nature05143>
- Durham, T.B., Toth, J.L., Klimkowski, V.J., Cao, J.X., Siesky, A.M., Alexander-Chacko, J. et al. (2015) Dual exosite-binding inhibitors of insulin-degrading enzyme challenge its role as the primary mediator of insulin clearance *in vivo*. *J. Biol. Chem.* **290**, 20044–20059, <https://doi.org/10.1074/jbc.M115.638205>
- Manolopoulou, M., Guo, Q., Malito, E., Schilling, A.B. and Tang, W.J. (2009) Molecular basis of catalytic chamber-assisted unfolding and cleavage of human insulin by human insulin-degrading enzyme. *J. Biol. Chem.* **284**, 14177–14188, <https://doi.org/10.1074/jbc.M900068200>
- McCord, L.A., Liang, W.G., Dowdell, E., Kalas, V., Hoey, R.J., Koide, A. et al. (2013) Conformational states and recognition of amyloidogenic peptides of human insulin-degrading enzyme. *Proc. Natl. Acad. Sci. U.S.A.* **110**, 13827–13832, <https://doi.org/10.1073/pnas.1304575110>
- Im, H., Manolopoulou, M., Malito, E., Shen, Y., Zhao, J., Neant-Fery, M. et al. (2007) Structure of substrate-free human insulin-degrading enzyme (IDE) and biophysical analysis of ATP-induced conformational switch of IDE. *J. Biol. Chem.* **282**, 25453–25463, <https://doi.org/10.1074/jbc.M701590200>
- Noinaj, N., Song, E.S., Bhasin, S., Alper, B.J., Schmidt, W.K., Hersh, L.B. et al. (2012) Anion activation site of insulin-degrading enzyme. *J. Biol. Chem.* **287**, 48–57, <https://doi.org/10.1074/jbc.M111.264614>
- Guo, Q., Manolopoulou, M., Bian, Y., Schilling, A.B. and Tang, W.J. (2010) Molecular basis for the recognition and cleavages of IGF-II, TGF- $\alpha$ , and amylin by human insulin-degrading enzyme. *J. Mol. Biol.* **395**, 430–443, <https://doi.org/10.1016/j.jmb.2009.10.072>



- 13 Perlman, R.K., Gehm, B.D., Kuo, W.L. and Rosner, M.R. (1993) Functional analysis of conserved residues in the active site of insulin-degrading enzyme. *J. Biol. Chem.* **268**, 21538–21544
- 14 Duckworth, W.C., Bennett, R.G. and Hamel, F.G. (1998) Insulin degradation: progress and potential. *Endocr. Rev.* **19**, 608–624
- 15 Farris, W., Mansourian, S., Chang, Y., Lindsley, L., Eckman, E.A., Frosch, M.P. et al. (2003) Insulin-degrading enzyme regulates the levels of insulin, amyloid  $\beta$ -protein, and the  $\beta$ -amyloid precursor protein intracellular domain *in vivo*. *Proc. Natl. Acad. Sci. U.S.A.* **100**, 4162–4167, <https://doi.org/10.1073/pnas.0230450100>
- 16 Camberos, M.C., Perez, A.A., Udrisar, D.P., Wanderley, M.I. and Cresto, J.C. (2001) ATP inhibits insulin-degrading enzyme activity. *Exp. Biol. Med. (Maywood)* **226**, 334–341, <https://doi.org/10.1177/153537020122600411>
- 17 Song, E.S., Juliano, M.A., Juliano, L., Fried, M.G., Wagner, S.L. and Hersh, L.B. (2004) ATP effects on insulin-degrading enzyme are mediated primarily through its triphosphate moiety. *J. Biol. Chem.* **279**, 54216–54220, <https://doi.org/10.1074/jbc.M411177200>
- 18 Duckworth, W.C. (1990) Insulin-degrading enzyme. In *Handbook of Experimental Pharmacology* (Cuatrecasas, P. and Jacobs, S., eds), pp. 143–165, Springer-Verlag
- 19 El Hage, K., Pandeyarajan, V., Phillips, N.B., Smith, B.J., Menting, J.G. and Whittaker, J. (2016) Extending halogen-based medicinal chemistry to proteins: Iodo-insulin as a case study. *J. Biol. Chem.* **291**, 27023–27041, <https://doi.org/10.1074/jbc.M116.761015>
- 20 Lommerse, J.P.M., Stone, A.J., Taylor, R.A. and Allen, F.H. (1996) The nature and geometry of intermolecular interactions between halogens and oxygen or nitrogen. *J. Am. Chem. Soc.* **118**, 3108–3116
- 21 Metrangolo, P., Neukirch, H., Pilati, T. and Resnati, G. (2005) Halogen bonding based recognition processes: a world parallel to hydrogen bonding. *Acc. Chem. Res.* **38**, 386–395, <https://doi.org/10.1021/ar0400995>
- 22 Politzer, P., Murray, J.S. and Clark, T. (2013) Halogen bonding and other  $\sigma$ -hole interactions: a perspective. *Phys. Chem. Chem. Phys.* **15**, 11178–11189, <https://doi.org/10.1039/c3cp00054k>
- 23 Linde, S., Sonne, O., Hansen, B. and Gliemann, J. (1981) Monoiodoinsulin labelled in tyrosine residue 16 or 26 of the insulin B-chain. Preparation and characterization of some binding properties. *Hoppe. Seylers Z. Physiol. Chem.* **362**, 573–579, <https://doi.org/10.1515/bchm2.1981.362.1.573>
- 24 Burant, C.F., Treutelaar, M.K., Peavy, D.E., Frank, B.H. and Buse, M.G. (1988) Differential binding of monoiodinated insulins to muscle and liver derived receptors and activation of the receptor kinase. *Biochem. Biophys. Res. Commun.* **152**, 1353–1360, [https://doi.org/10.1016/S0006-291X\(88\)80434-0](https://doi.org/10.1016/S0006-291X(88)80434-0)
- 25 Pandeyarajan, V., Phillips, N.B., Cox, G.P., Yang, Y., Whittaker, J., Ismail-Beigi, F. et al. (2014) Biophysical optimization of a therapeutic protein by nonstandard mutagenesis: Studies of an iodo-insulin derivative. *J. Biol. Chem.* **289**, 23367–23381, <https://doi.org/10.1074/jbc.M114.588277>
- 26 Noinaj, N., Bhasin, S.K., Song, E.S., Scoggin, K.E., Juliano, M.A., Juliano, L. et al. (2011) Identification of the allosteric regulatory site of insulin-degrading enzyme. *PLoS ONE* **6**, e20864, <https://doi.org/10.1371/journal.pone.0020864>
- 27 da Cruz, C.H. and Seabra, G. (2014) Molecular dynamics simulations reveal a novel mechanism for ATP inhibition of insulin degrading enzyme. *J. Chem. Inf. Model.* **54**, 1380–1390, <https://doi.org/10.1021/ci400695m>
- 28 Sharma, S.K., Chorell, E., Steneberg, P., Vernersson-Lindahl, E., Edlund, H. and Wittung-Stafshede, P. (2015) Insulin-degrading enzyme prevents  $\alpha$ -synuclein fibril formation in a nonproteolytic manner. *Sci. Rep.* **5**, 12531, <https://doi.org/10.1038/srep12531>
- 29 Sorci, M., Grassucci, R.A., Hahn, I., Frank, J. and Belfort, G. (2009) Time-dependent insulin oligomer reaction pathway prior to fibril formation: cooling and seeding. *Proteins* **77**, 62–73, <https://doi.org/10.1002/prot.22417>
- 30 Gerstein, A.S. (2001) Nucleotides, oligonucleotides, and polynucleotides. In *Molecular Biology Problem Solver: A Laboratory Guide* (Gerstein, A.S., ed.), pp. 267–289, Wiley-Liss, Inc
- 31 Zheng, Q. and Lazo, N.D. (2018) Mechanistic studies of the inhibition of insulin fibril formation by rosmarinic acid. *J. Phys. Chem. B* **122**, 2323–2331, <https://doi.org/10.1021/acs.jpcc.8b00689>
- 32 Lazo, N.D. and Downing, D.T. (1997) Circular dichroism of model peptides emulating the amphipathic  $\alpha$ -helical regions of intermediate filaments. *Biochemistry* **36**, 2559–2565, <https://doi.org/10.1021/bi963061b>
- 33 Chesneau, V. and Rosner, M.R. (2000) Functional human insulin-degrading enzyme can be expressed in bacteria. *Protein Expr. Purif.* **19**, 91–98, <https://doi.org/10.1006/prep.2000.1217>
- 34 Bar-Even, A., Noor, E., Savir, Y., Liebermeister, W., Davidi, D., Tawfik, D.S. et al. (2011) The moderately efficient enzyme: evolutionary and physicochemical trends shaping enzyme parameters. *Biochemistry* **50**, 4402–4410, <https://doi.org/10.1021/bi2002289>
- 35 Hammes, G.G. (2002) Multiple conformational changes in enzyme catalysis. *Biochemistry* **41**, 8221–8228, <https://doi.org/10.1021/bi0260839>
- 36 Krasinski, C.A., Zheng, Q., Ivancic, V.A., Spratt, D.E. and Lazo, N.D. (2018) The longest amyloid- $\beta$  precursor protein intracellular domain produced with A $\beta$ 42 forms  $\beta$ -sheet-containing monomers that self-assemble and are proteolyzed by insulin-degrading enzyme. *ACS Chem. Neurosci.*, <https://doi.org/10.1021/acschemneuro.8b00305>
- 37 Lazo, N.D., Grant, M.A., Condrón, M.C., Rigby, A.C. and Teplow, D.B. (2005) On the nucleation of amyloid  $\beta$ -protein monomer folding. *Protein Sci.* **14**, 1581–1596, <https://doi.org/10.1110/ps.041292205>
- 38 Grant, M.A., Lazo, N.D., Lomakin, A., Condrón, M.M., Arai, H., Yamin, G. et al. (2007) Familial Alzheimer's disease mutations alter the stability of the amyloid  $\beta$ -protein monomer folding nucleus. *Proc. Natl. Acad. Sci. U.S.A.* **104**, 16522–16527, <https://doi.org/10.1073/pnas.0705197104>
- 39 Liu, G., Prabhakar, A., Aucoin, D., Simon, M., Sparks, S., Robbins, K.J. et al. (2010) Mechanistic studies of peptide self-assembly: Transient  $\alpha$ -helices to stable  $\beta$ -sheets. *J. Am. Chem. Soc.* **132**, 18223–18232, <https://doi.org/10.1021/ja1069882>
- 40 Bellia, F., Pietropaolo, A. and Grasso, G. (2013) Formation of insulin fragments by insulin-degrading enzyme: the role of zinc(II) and cystine bridges. *J. Mass Spectrom.* **48**, 135–140, <https://doi.org/10.1002/jms.3060>
- 41 Grasso, G., Rizzarelli, E. and Spoto, G. (2009) The proteolytic activity of insulin-degrading enzyme: a mass spectrometry study. *J. Mass Spectrom.* **44**, 735–741, <https://doi.org/10.1002/jms.1550>
- 42 Patel, A., Malinowska, L., Saha, S., Wang, J., Alberti, S., Krishnan, Y. et al. (2017) ATP as a biological hydrotrope. *Science* **356**, 753–756, <https://doi.org/10.1126/science.aaf6846>

- 43 Lazo, N.D., Maji, S.K., Fradinger, E.A., Bitan, G. and Teplow, D.B. (2005) The amyloid- $\beta$  protein. In *Amyloid Proteins: The Beta Sheet Conformation and Disease* (Sipe, J.C., ed.), pp. 385–491, Wiley-VCH
- 44 Swerdlow, R.H. (2011) Brain aging, Alzheimer's disease, and mitochondria. *Biochim. Biophys. Acta* **1812**, 1630–1639, <https://doi.org/10.1016/j.bbadis.2011.08.012>
- 45 Wang, X., Su, B., Lee, H.G., Li, X., Perry, G., Smith, M.A. et al. (2009) Impaired balance of mitochondrial fission and fusion in Alzheimer's disease. *J. Neurosci.* **29**, 9090–9103, <https://doi.org/10.1523/JNEUROSCI.1357-09.2009>